X-660-77-144

TMX-71335

PREPRINT

X-RAY AND GAMMA RAY LINE PRODUCTION BY NONTHERMAL IONS

R. W. BUSSARD
K. OMIDVAR
R. RAMATY

JUNE 1977

GSFC — GODDARD SPACE FLIGHT CENTER —
GREENBELT, MARYLAND

X-RAY AND GAMMA-RAY LINE PRODUCTION BY NONTHERMAL IONS

R. W. Bussard* and R. Ramaty
Laboratory for High Energy Astrophysics
NASA/Goddard Space Flight Center
Greenbelt, Maryland 20771

and

K. Omidvar
Laboratory for Planetary Atmospheres
NASA/Goddard Space Flight Center
Greenbelt, Maryland 20771

*Also Department of Physics and Astronomy, University of Maryland
College Park, Maryland

ABSTRACT

We have calculated X-ray production at $\sim$ 6.8 keV by the 2p to 1s transition in fast hydrogen- and helium-like iron ions, following both electron capture to excited levels and collisional excitation. We used a refinement of the OBK approximation to obtain an improved charge exchange cross-section. This, and the corresponding ionization cross-section were used to determine equilibrium charge fractions for iron ions as functions of their energy. The effective X-ray line production cross-section was found to be sharply peaked in energy at about 8 to 12 MeV/amu. Since fast ions of similar energies can also excite nuclear levels, we have calculated the ratio of selected strong γ-ray line emissivities to the X-ray line emissivity. We use these calculations to set limits on the intensity of γ-ray line emission from the galactic center and the radio galaxy Centaurus A, and we find that these limits are generally lower than those reported in the literature.

I. INTRODUCTION

A flux of fast subrelativistic ions in a medium can produce line emission in both the X-ray and the γ-ray regions. This paper is concerned with the production of the lines of the 2p to 1s transitions in hydrogen- and helium-like iron ions (at $\sim$ 6.8 keV), and with the comparison of these lines with the strong γ-ray line at 4.44 MeV resulting from the nuclear deexcitation of ^{12}C. The 2p to 1s transitions in more abundant species such as C, N and O give rise to less energetic X-ray photons, which subsequently suffer interstellar absorption.

The X-ray calculations presented in this paper are similar to those of Pravdo and Boldt (1975) who have treated X-ray line produc-

tion from energetic oxygen nuclei in the interstellar medium. Watson (1975) has calculated the multiplicities of X-rays produced by fast iron and oxygen nuclei interacting with ambient hydrogen, but as we shall show, interstellar oxygen and iron, and not hydrogen, are the main contributors to electron capture by fast iron ions. By using improved cross sections for charge exchange and excitation, we have carried out a detailed calculation of X-ray line production from fast ions moving through an ambient medium with solar system abundances.

Astrophysical γ-ray line production has been investigated by Ramaty, Kozlovsky and Lingenfelter (1975) and Ramaty, Kozlovsky and Suri (1977) for solar flares, and by Meneguzzi and Reeves (1975) and Lingenfelter and Ramaty (1977) for the interstellar medium. By combining these results with the calculated X-ray line emission, we evaluate ratios of the X-ray and γ-ray line intensities. These can be used to set limits on the expected γ-ray line emission from various source regions for which X-ray observations are available. We note that iron line emission has been observed from several sources (Pravdo et al. 1976, Mitchell et al. 1976, Serlemitsos et al. 1977) but this emission is likely to be thermal. Thus, only upper limits are available at the present time on the intensity of the $\sim$ 6.8 keV line from nonthermal particles.

II. X-RAY PRODUCTION

a) Charge Exchange, Excitation and Ionization Cross Sections

We consider energetic (about 1 to 300 MeV/amu) Fe ions moving through an ambient medium with solar abundances (Cameron 1973,

except for the abundance of He for which we use the results of Brown and Lockman 1976). The 2p to 1s transitions in such ions having one or two bound electrons give rise to $K\alpha$ X-rays at 6.9 and 6.7 keV, respectively. Because of Doppler broadening, however, these 2 lines merge into a broad feature centered at about 6.8 keV. For bare nuclei, the 2p state can be populated by charge exchange with ambient atoms; for ions having one electron, the 2p state can be populated by charge exchange or excitation; and for ions having 2 electrons, the 2p to 1s transition can only occur following excitation.

The method for calculating the charge exchange cross-sections for bare Fe nuclei, a refinement of the OBK approximation, is described in the appendix. The results at five energies, tabulated by the species of target atom, are shown in Table 1. The three rows for each target element give the capture cross sections to any state which subsequently deexcites to the 1s, 2p and 2s levels, respectively.

The charge exchange cross sections which lead to electrons in the 2p level are shown in Figure 1 as functions of the temperature of the ambient medium for the 5 energies given in Table 1. At low temperatures ($< 5 \times 10^5$K) these cross sections are the same as those given in Table 1. The cross sections decrease with increasing temperature because the target atoms lose some of their orbital electrons. We have estimated the temperature dependences shown by folding together the contribution of the partial cross sections for charge exchange from each electronic orbital and the ionization fractions at a given temperature. For these partial cross sections we used the calculations described in the appendix, while the ionization fractions are from J. C. Raymond (private communication 1977). The

results indicate that the cross sections are fairly constant up to a gas temperature of a few hundred thousand degrees, but fall off rapidly with increasing temperature. It should be noted that the temperature dependences shown in Figure 1 might require some modification since the partial cross sections were obtained for neutral targets. In subsequent calculations, however, we only use the cross section at low temperatures where the targets which are the major contributors to charge exchange are mostly neutral. This cross-section is shown as a function of energy by the dotted line in Figure 2.

The cross-section for excitation of a hydrogen-like ion from the 1s to the 2p level is given by:

$$\sigma_{exc}(Z) = \frac{2^{18} Z_m^2 \pi A_o^2}{\left(\frac{m_e}{m_p}\frac{E}{I_H}\right)^2} \int_{t_{min}}^{\infty} \frac{dt}{t^3}\left[1 - \frac{16\, Z_m^3}{(4Z_m^2 + t^2)^2}\right]\left[\frac{3\,\frac{t}{Z}}{\left(4\,\frac{t^2}{Z^2} + 9\right)^3}\right]^2, \qquad (1)$$

(Bates 1962). Here Z_m is the atomic number of the gas atom causing excitation, A_o is the Bohr radius (.529Å), and Z is the charge, in units of the electron charge, of the ion being excited. Also, m_e and m_p are the electron and proton masses, respectively, E is the kinetic energy per nucleon of the projectile, and I_H is the ionization potential of hydrogen (13.6 eV). The lower limit on the integral, t_{min}, is given by

$$t_{min} = \frac{\Delta E}{2}\sqrt{\frac{m_p}{m_e I_H E}}\left(1 + \frac{m_p}{4M}\frac{\Delta E}{E}\right), \qquad (2)$$

where ΔE is the difference in energy between the two levels, and M is the reduced mass for the encounter.

The ionization cross-section of iron ions in collisions with ambient neutral hydrogen were taken from Watson (1975), but since he considered a gas consisting only of hydrogen, we have scaled his cross-sections to account for the effects of helium. There are two contributions to these cross-sections: one in which the target atom is not itself excited, called the elastic part, and an inelastic part, which includes the sum over all possible excitations of the target (e.g. Rule 1977). For iron projectiles on hydrogen and helium, each part contributes almost equally, but the elastic part scales as the target charge squared, while the inelastic part varies linearly with the target charge. Also we compared the calculations of Rule (1977) with the Watson (1975) cross-section for ionization of the hydrogen-like iron and found good agreement.

Since the energy required to ionize the iron projectiles is so large compared to the target ionization potentials, the ionizing collisions take place at very small impact parameters. Thus, electronic screening of the target nuclei is not very important, and these same results should apply to an ionized medium. In fact, Rule (1977) calculated the ionization cross-sections for both cases, and found differences of $\leq$ 10% for the energies under consideration.

b) Effective X-ray Production Cross Sections

The effective X-ray production cross-sections were obtained by folding the cross-sections for capture and excitation with the appropriate charge fractions:

$$\sigma_c(2p) = f_o\,\sigma_c^{(o)}(2p) + f_1\sigma_c^{(1)}(2p),$$
$$\sigma_{exc} = f_1\,\sigma_{exc}^{(1)} + f_2\,\sigma_{exc}^{(2)} \qquad (3)$$
$$\sigma_c(2s) = \frac{3}{4}\,f_1\,\sigma_c^{(1)}(2s)$$

where σ_c (2p) is the effective cross-section for X-ray production following the capture of an electron which cascades through the 2p to 1s levels, $\sigma_c^{(n)}$(2p or 2s) is the cross-section for the capture of an electron into the 2p or 2s level, either directly or following a cascade, by an ion which already has n electrons, σ_{exc} is the X-ray production cross-section following excitation , and $\sigma_{exc}^{(n)}$ is the cross-section for excitation of an ion with n electrons. The cross sections $\sigma_c^{(n)}$ are obtained by multiplying the cross sections given in Table 1 by $(Z_{eff}/26)^5$, where Z_{eff} is the bare charge corrected for electronic screening. The screening effect was taken from Burns (1964) for all the cross sections considered. The 2s term represents the magnetic dipole transition, which occurs more rapidly than two photon emission only in the triplet state of the helium-like ion. On the average, this state is populated 3 times more often than the singlet state, giving rise to the factor 3/4. The f_n are the charge fractions or the fractions of all ions with n electrons.

The charge fractions satisfy the equation:

$$\frac{\partial f_n}{\partial} + \frac{\partial}{\partial E}\left(f_n \frac{dE}{dt}\right) = n_H\, v(\sigma_c^{(n-1)} f_{n-1} - \sigma_I^{(n)} f_n + \sigma_I^{(n+1)} f_{n+1} - \sigma_c^{(n)} f_n), \qquad (4)$$

where the subscript I refers to ionization, n_H is the hydrogen density, v the projectile velocity, and $\frac{dE}{dt}$ is the time rate of energy loss. In a steady state situation and if the energy losses are slow

compared to charge exchange and ionization collisions, equation 4 reduces to

$$f_n \sigma_c^{(n)} = f_{n+1} \sigma_I^{(n+1)} \tag{5}$$

For this equation to be valid, the time between collisions represented by terms on the right side of equation 4 should be much shorter than the energy loss time of the ions. Since the charge exchange collisions manifest themselves in X-ray production, we expect that this condition will be satisfied when the X-ray multiplicity, defined by

$$N = (n_H/\rho) \int_o^E dE \, \sigma_x/(dE/dx) \tag{6}$$

is much larger than unity. Here ρ is the gas mass density, $\sigma_x = \sigma_c(2p) + \sigma_{exc} + \sigma_c(2s)$ is the total 6.8 keV X-ray production cross-section from equation 3, dE/dx is the energy per amu lost per g cm^{-2} of matter traversed, and E is some energy at which the ions are essentially bare. In evaluating equation (6) we assume that the Fe ion is in charge equilibrium at all energies. The energy loss rate dE/dx in a neutral medium was taken from the tabulations of Barkas and Berger (1964) and Northcliffe and Schilling (1970), for a gas composed of H and He with 8.5% He by number. The effective charge for the Fe ions was taken from Northcliffe and Schilling (1970). The losses of fast ions in an ionized medium were calculated by using

$$\frac{dE}{dx} = - \frac{2\pi e^4 Z^2 n_e}{m_e v} \left(\ln \frac{m_e^3 v^4}{\pi e^2 n_e h^2} \right), \tag{7}$$

Ginsburg and Syrovatskii 1964), where e and m are the electron

charge and mass, Ze the ion charge, v is the velocity of the ion, and n_e is the electron density, taken equal to the hydrogen density.

Table 2 shows the multiplicity of ~ 6.8 keV X-rays as evaluated from equation (6) for several values of E. For a neutral medium, the multiplicity is high enough that equation (5) should be a good approximation. However, in an ionized medium the multiplicity is low, and hence equation (5) may not be a good approximation. An exception is the case of continuous acceleration where another term is added to equation (4) to cancel the effects of the energy losses. But even if such acceleration is not present, we would still expect about one X-ray photon per each energetic iron ion. Since the multiplicity for the ionized case in Table 2 is already close to unity, we do not expect that the use of equation (5) will lead to any substantial error, even in this case.

Figure 3 shows the charge fractions as functions of the projectile kinetic energy per nucleon, calculated by using equation (5). It shows that on the average, the iron nuclei are bare above ~ 40 MeV/amu, that they have picked up one electron by ~ 14 MeV/amu, that they have two electrons by ~ 10 MeV/amu. Below about 6 MeV/amu, the average iron ion has 3 or more electrons. When this happens, the outer electron usually takes the energy from collisions, so the $K\alpha$ transition occurs rarely from ions with 3 or more electrons.

The charge fractions shown in Figure 3 were then used to weight the cross-sections discussed in section IIa, according to equations (3). The results are shown in Figure 2 as the solid lines. Both curves show the same energy dependence, and excitation is seen to be

the dominant mechanism for X-ray line production. Both cross-sections are fairly sharply peaked in energy at around 10 MeV/amu. Because of the sharpness of the peak, we estimate the width of the broad 6.8 keV feature to be $\simeq$ 2.4 keV. Also, observation of this line will give the amount of iron with energy from approximately 5 to 20 MeV/amu in the source. This number is about 10^{-44} $M_\odot$ of iron per photon per sec produced, for a hydrogen density of 1 cm^{-3}, and varies little with the assumed spectrum of ions ($\pm \sim$ 50% over the spectra considered in this paper).

III. RESULTS

We have integrated the X-ray production cross-sections shown in Figure 2 over a variety of spectra of fast ions. The abundances of these ions were extrapolated from measurements at $\geq$ 300 MeV/amu (e.g. Meyer, Ramaty, Webber, 1974), H: He: C: N: O: Fe = 1: .1: 5.6×10^{-3}: 2.8×10^{-3}: 5.4×10^{-3}: 5×10^{-4} and taken to be independent of energy. The spectra used for all species are power laws in kinetic energy per amu with a low energy cutoff, E_c:

$$n(E) \propto \begin{cases} E^{-s} & \text{for } E \geq E_c \\ \text{constant} & \text{for } E < E_c \end{cases}, \qquad (8)$$

where n(E) is the number density of ions per interval of kinetic energy/amu. We have also set n(E) equal to zero for E>300 MeV. As mentioned above the gas abundances used were taken from Cameron (1973), with the exception of He (Brown and Lockman 1976). They are given in Table 1.

Figure 4 shows the 6.8 keV line emissivity per H atom for an energy content of 1 eV cm^{-3} in fast ions from 1 to 300 MeV/amu.

It can be seen that the spectra which maximize X-ray production have breaks at around 10 MeV/amu and fall off rapidly above that energy. This is a result of the sharp maximum in the X-ray production cross section at around 10 MeV/amu, shown in Figure 2.

Figure 5 shows the ratio of 6.8 keV photons produced to the energy deposited in the gas by the fast ions. Here, the X-ray line emission is maximized with respect to energy deposited when the spectrum has a break at about 15 MeV/amu. The curves are shown for both a neutral and an ionized gas. They have the same shapes for both types of medium, but since energy is lost faster in a plasma owing to collective long range interactions (emission of plasma waves) the curves are displaced downward in an ionized gas.

In addition to the X-ray lines of iron, ions in the energy range under consideration will cause nuclear reactions, with subsequent γ-ray line emission. Meneguzzi and Reeves (1975) and Ramaty, Kozlovsky and Lingenfelter (1975) have shown that in these reactions the strongest line is at 4.44 MeV. This line has two components. One is narrow, resulting from gas nuclei excited by fast H and He, and the other is broad, from the excitation of the fast nuclei by ambient H and He. Since we are assuming different relative abundances of heavy nuclei in the gas and the fast particles, these two components have unequal intensities, and hence are treated separately in the present paper. For the calculation of both the narrow and broad 4.44 MeV line intensities, we use the cross section compiled by Ramaty, Kozlovsky and Suri (1977). In addition, we also include the broad

component of the 0.85 MeV line of ^{56}Fe, since this line intensity scales directly with the amount of fast iron which produce the broad $\sim$ 6.8 keV X-ray line.

In Figure 6, we show ratios of γ-ray to X-ray line emissivities, $q_\gamma/q(6.8)$, calculated for the equilibrium case, for the two components of the carbon-line and the broad component of the iron γ-ray line. In addition to the effects of direct excitation of carbon by hydrogen and helium, we have also included the contribution of spallation of nitrogen and oxygen to the excited carbon nucleus. The X-ray production scales directly with the relative abundance of iron in the fast ions, but varies in a more complicated way with the relative abundances of heavy nuclei in the gas, primarily iron and oxygen. On the other hand, the broad component of γ-radiation scales with the relative abundance of fast C, N and O ions, and the narrow component scales with the gas abundances of these nuclei. Thus, the ratio of γ-ray to X-ray yields depends somewhat on the relative abundances of medium and heavy nuclei. For example, by increasing the abundances of C and heavier nuclei in both the gas and fast particles by a factor of 10, the 4.44-MeV γ-ray intensity also increases by a factor of 10, but the $\sim$ 6.8 keV X-rays increase by about a factor of 20, and hence $q_\gamma/q(6.8)$ decreases by a factor of 2.

Figure 6 shows that there is less than an order of magnitude of variation of $q_\gamma/q(6.8)$ with spectrum, except for spectra which flatten at $\geq$ 50 MeV/amu. The flatter spectra favor γ-ray emission because the cross-sections for nuclear excitation drop off much more slowly at high energies than does the X-ray production cross-section. This trend is also reflected in the fact that lower spectral indices favor γ-ray emission. Since we have assumed a high energy cutoff at 300 MeV/amu,

we do not take into account line emission or γ rays from π^0 decay produced by particles at higher energies.

IV. APPLICATIONS TO THE GALACTIC CENTER, CEN A, AND CAS A

We now apply the results of the previous section to examine the consistency of the reported γ-ray data from the galactic center region and the radio galaxy Centaurus A (Haymes et al. 1975, Hall et al. 1976) with upper limits on the nonthermal 6.8 keV line from these sources (Kellogg et al. 1971, R. Mushotzky, private communication 1977). We also set limits on the flux of energetic particles in the supernova remnant Cassiopeia A by using upper limits on the broad X-ray line emission from this source (P. J. Serlemitsos, private communication).

Haymes et al (1975) have claimed to see a feature at around 4.6 MeV from the direction of the galactic center which they attributed to the 4.44 MeV line of ^{12}C. The opening angle of the γ-ray detector used was 13^o (FWHM). From the observations of Kellogg et al. (1971) of the X-ray sources GCX at the galactic center, we take the measured flux of 1.1×10^{-2} photons $cm^{-2}s^{-1}$ in a 2.4 keV band centered at 6.8 keV as an upper limit on the intensity of the broad iron Kα line from GCX. Using this upper limit, we have set upper limits on both the broad and narrow γ-ray lines produced by fast ions in GCX. Under the most favorable conditions for γ-ray production considered ($s = 1.2$, $E_c = 100$ MeV/amu, see Figure 6) the upper limits on the narrow and broad components are 3.2×10^{-5} and 3.3×10^{-4} photons $cm^{-2}s^{-1}$, respectively. Haymes et al. (1975) give an intensity of $(9.5 \pm 2.7) \times 10^{-4}$ photons $cm^{-2}s^{-1}$ with a width of several hundred keV, so they could have

been observing the broad component. In this case, our upper limit is a factor of three below their observation. Since the opening angle of the γ-ray detector is larger than the angle subtended by GCX, we examined data from the Goddard Cosmic X-Ray Spectroscopy Experiment on board OSO-8 (Pravdo et al. 1976) to obtain the X-ray flux from an area of 13^{o}x13^{o} centered on GCX. Here, the upper limit to a broad 6.8 keV feature is $2.4\text{x}10^{-2}$ photons $cm^{-2}s^{-1}$, which implies upper limits of $7.4\text{x}10^{-4}$ and $7.3\text{x}10^{-5}$ photons $cm^{-2}s^{-1}$ to the broad and narrow γ-ray components, respectively. Thus the observation of Haymes et al. (1975), provided they indeed represent the broad γ-ray component and their source is larger than GCX, is not inconsistent with the upper limits set by the X-ray data. However, as we shall now discuss, the energy density in energetic particles required to account for the γ-ray data under the constraints of the X-ray upper limits is much larger than the limits set by the distribution of gas perpendicular to the plane in the galactic center region.

The energy density in fast ions required to produce a ~ 6.8 keV X-ray flux of $2.4\text{x}10^{-2}$ photons $cm^{-2}s^{-1}$ for s = 1.2 and E_c = 100 MeV/amu is, from Figure 4, $2\text{x}10^{11}/M_H$ eV cm^{-3}, where M_H is the mass of hydrogen in the source, in solar masses. Scoville, Solomon, and Jefferts (1974) and Mezger (1974) have estimated that the amount of gas in the nuclear region is some 10^7 to 10^8 $M_\odot$, and so, the above γ-ray flux requires several keV cm^{-3} in fast ions. This energy density is 2 orders of magnitude larger than that required to maintain the z distribution of gas at the galactic center (Sanders and Wrixon 1973). We could lower this energy density in a manner similar to that suggested by Lingenfelter and Ramaty (1976). They proposed that the abundances

of C and heavier nuclei relative to H in both the ambient gas and energetic particles could be larger than solar and cosmic ray abundances, and they assumed spectral parameters for the energetic particles which maximize the γ-ray line emission with respect to energy content ($s \geq 3$, $E_c \simeq 15$ MeV/amu). However, both these assumptions lower $q_\gamma/q(6.8)$. As can be seen from Figure 6, for ($s = 3$, $E_c = 15$ MeV/amu) $q_\gamma/q(6.8)$ is lower by about an order of magnitude than for ($s = 1.2$, $E_c = 100$ MeV/amu). Furthermore, since $q(6.8)$ depends on the relative abundances of the heavy nuclei in both the gas and the energetic particles, while q_γ depends on these relative abundances in only one component, an increase of heavy nuclei abundances decreases $q_\gamma/q(6.8)$. Therefore, we conclude that it is difficult to lower substantially the energy density required to produce the γ-ray flux observed by Haymes et al. (1975) without leading to conflict with the X-ray data. The only exceptions could arise if the source region is hot so that the charge exchange and X-ray production are suppressed, or that it is opaque to the X-rays but not to the gamma rays.

We note, from Figure 5, that to produce a 6.8 keV X-ray flux of 2.4×10^{-2} photons $cm^{-2} sec^{-1}$, the energy deposited in a neutral gas by the energetic particles with spectrum $s = 1.2$ and $E_c = 100$ MeV is about 2×10^{42} erg/sec. This energy release is large, but still of the same order as the observed far infrared luminosity of the galactic center (Hoffman, Frederick, and Emery, 1971). The energy deposited in an ionized gas is larger by a factor of 5 than that in a neutral gas.

If, nonetheless, we use the spectral parameters $s = 3$ and

E_c = 15 MeV/amu, we find that the observed upper limit on the broad 6.8 keV line from a $13^o x 13^o$ region implies, from Figure 6, upper limits of 10^{-5} and 10^{-4} photons $cm^{-2}s^{-1}$ on the narrow and broad 4.44-MeV line intensities. For these fluxes the energy density in fast ions is, from Figure 4, only $4x10^9/M_H$, a factor of 50 less than that required to account for the observations of Haymes et al. (1975).

In addition to the galactic center, γ-radiation was also detected from Centaurus A (Hall et al., 1976). They claimed a feature at 4.5 MeV, most likely less broad than $\sim$ 150 keV, at a confidence level of 3.3σ, with a line flux of $(9.9 \pm 3.0)x10^{-4}$ photons $cm^{-2}s^{-1}$. We examined the X-ray spectrum of Cen A around 6.8 keV (R. Mushotzky, private communication), and placed an upper limit of $8.1x10^{-3}$ photons $cm^{-2}s^{-1}$ on the broad Fe Kα flux. Again, using the most favorable spectrum for γ-ray production, we obtained upper limits of $2.5x10^{-5}$ and $2.6x10^{-4}$ photons $cm^{-2}s^{-1}$ to the narrow and broad 4.44 MeV components, respectively. Thus, the upper limit on the narrow component is a factor of 40 below the observation. Because of the quoted width of the $\sim$ 4.5 MeV feature from Cen A, it is unlikely that this feature is the broad 4.44 MeV line.

Since supernovae or supernova remnants are candidates for sites of particle acceleration, we examined the spectrum of Cas A, a young supernova remnant. Because of a narrow thermal line at 6.7 keV (Pravdo et al. 1976), we used for an upper limit on flux in a broad line the flux above continuum at 4.85 keV (P. J. Serlemitsos, private communication 1977). This was fit to a gaussian centered at 6.8 keV

and a full width at half maximum of 2.4 keV and gave an upper limit of 7×10^{-3} photons $cm^{-2} s^{-1}$ in the broad line. At an assumed distance of 3 kpc, we obtain for the mass of Fe in the energy range 5 to 20 MeV/amu, as discussed in section II b, $< 0.1/n_H \; M_\odot$, where n_H is the atomic hydrogen density at the source. From Figure 6, we can set upper limits on the broad and narrow components of the 4.44 MeV ^{12}C line of 2.8×10^{-4} and 2.7×10^{-5} photons $cm^{-2} s^{-1}$, respectively. Presently planned γ-ray experiments could detect such fluxes, and thus we expect to obtain even more meaningful limits on the fluxes of energetic ions in supernova remnants from these experiments.

V. CONCLUSIONS

Using detailed cross-sections for charge exchange, ionization, and excitation, we have calculated the production rate of Kα X-rays from subrelativistic iron ions. After assuming a set of abundances and energy spectra for these ions, we presented X-ray line production rates for both a given energy density and a given energy deposition rate of the energetic particles. Then, we compared these results with the rate of γ-ray production from the first excited levels of ^{12}C and ^{56}Fe. In section IV, these calculations were applied to the galactic center, Cen A, and Cas A. For the galactic center, the reported observation of the 4.44 MeV line (Haymes et al. 1975) are not inconsistent with upper limits on the broad 6.8 keV line. However, this consistency with the X-ray data implies that the energy density in fast ions required to produce the observed gamma rays is several keV cm^{-3}. In the case of Cen A, Hall et al. (1976) reported a feature at $\sim$ 4.5 MeV with a width of $\leq$150 keV. The

intensity of this feature is a factor of 40 larger than the upper limit on a narrow ^{12}C line set by the X-ray data. We note, however, that the constraints on gamma-ray line intensities imposed by upper limits on broad 6.8 keV emission do not apply to sources that are either hotter than a million degrees or opaque to the 6.8 keV photons. Thus, the future detection either of nuclear γ-ray line emission or of a broad 6.8 keV X-ray line, or both, could give very valuable information on the existence of fast ions in the interstellar medium and on the physical conditions that lead to the production of these particles.

ACKNOWLEDGEMENTS

We gratefully acknowledge S. H. Pravdo and E. A. Boldt for stimulating discussions, D. W. Rule for assistance in evaluating cross sections, P. J. Serlemitsos, J. H. Swank, and R. H. Becker for assistance with the OSO-8 X-ray data, and E. C. Sullivan for programming the numerical evaluation of the cross sections. The research of R. W. Bussard was supported by NASA Grant 21-002-316 at the University of Maryland.

APPENDIX

BARE NUCLEI-MULTIELECTRON ATOMS CHARGE EXCHANGE

We have calculated the charge exchange cross section when a bare nucleus of charge $+z_1e$ captures an electron from a multi-electron atom. The state of the electron within each atomic shell is specified by $n_2l_2j_2m_{j_2}$, where n_2 is the principal quantum number, l_2 and j_2 are the orbital and total angular momenta quantum numbers of the electron, and m_{j_2} is the projection quantum number of j_2. After the capture the state of the electron is specified by $n_1l_1m_1$, with $n_1l_1m_1$ having the familiar meanings.

At present there are no reliable methods for calculating the bare nuclei-multielectron atoms charge-exchange cross sections. Nikolaev (1967) found that an approximation applied to charge exchange originally by Oppenheimer (1928) and Brinkman and Kramers (1930) predicts more or less accurately the shape of the experimental cross section curve versus energy, but the calculated cross sections were larger by a factor of 2-4 than the experimental cross sections. Nikolaev brings the OBK cross sections in rough agreement with the measurement by multiplying these cross sections by an empirical energy dependent factor. It has been shown (Omidvar et al 1976) that this semi-empirical method gives cross sections comparable in accuracy with those of more complicated but purely theoretical calculations.

Due to the complexity of other methods, especially when capture into the excited states are involved, here we have used the OBK approximation and have multiplied the cross sections by Nikolaev's empirical factor.

In the present calculation the projectile is described as a

structureless charged particle. The target atom is described by a model in which each electron in a given shell is in a central Coulomb field with an effective charge given by the Hartree-Fock calculations (Froese Fischer 1966). To account to some extent for the fact that the potential fields of the multielectron atoms are non-Coulombic, the measured, instead of the hydrogenic, ionization potentials have been used for the bound electrons. Thus each bound electron is specified by the three quantum numbers $n_2 l_2 j_2$, by the degenerate quantum number m_{j_2}, by the effective charge $+z_2 e$, and by the ionization potential.

Such a model for the target atom has been used with success for the inner shell ionization of atoms by heavy charged particles (Merzbacher and Lewis 1958). A similar model has been used for charge exchange by Nikolaev (1967). The use of the experimental, instead of the hydrogenic, ionization potential makes the prior and post forms of the exchange amplitudes (Messiah 1966) different from each other. Numerically we have found that for different $n_2 l_2 j_2 \rightarrow n_1 l_1$ transitions, and different energies, sometimes the prior cross sections are larger, and sometimes the post. The two forms usually differ by about 25% from each other, and occasionally they differ by as much as 50%. In the present calculation we have used the average of the two forms. The discrepancy between the two forms can be taken as a measure of the accuracy of the calculation.

When the charge of the bare nucleus exceeds unity, the final products of the charge exchange reactions are charged particles. The final state wave function then should be given asympotically by a Coulomb wave function, while in the present calculation a plane wave

for the final state has been used. Bates and Boyd (1962) have shown, however, that for projectile energies larger than 100 eV/amu the substitution of the plane wave for the Coulomb wave makes insignificant differences.

The charge exchange cross section has a strong dependence on the charge of the projectile, the effective charge of the target, and the projectile's energy. According to the Landau-Zener or adiabatic theory, valid for very low projectile-target relative velocities, the cross section increases with respect to the projectile's charge $z_1 e$ as z_1 (Olson and Salop 1976). According to the OBK approximation, valid at high energies, this dependence is z_1^5.

The dependence of the cross section on the effective charge of the target nucleus, $z_2 e$, is similarly strong at high energies. For $v \gg z_2 v_o$, where v is the relative velocity, and $v_o = e^2/h = \alpha c$ is the Bohr velocity, and α is the fine structure constant, the cross section increases as $Z_2^{5+2\ell}$ with ℓ the angular momentum quantum number of the electron before capture. For energies 5-30 MeV/nucleon considered here we find that for capture from s, p, and d states the powers of z_2 according to which the capture cross section increases are approximately 1-5, 5-7, and 8-9, respectively; the power increasing monotonically with respect to the energy.

The dependence on the energy is also of some interest. For the non-resonance exothermic charge transfer cross section of interest here, the cross section is finite for zero projectile energy, and it has slow variation with energy for low projectile energy. For energies higher than $\sim$ 1 MeV/amu, the cross section decreases as different negative powers of energies.

The target atoms considered are H, He, C, N, O, Ne, Mg, Si, S, and Fe. Electron capture from all the atomic shells, as described above, have been taken into account. This is the first calculation of its kind where capture from shells other than the 1s shell is taken into account. The Lyman α radiation is mostly due to the formation of Fe^{+25} (2p) as well as the formation of the higher excited state of Fe^{+25} and the consequent cascading to the 2p level.

In the present calculation cross sections for formation of Fe^{+25} (n_1,l_1), $2\leq n_1\leq 20$, $0\leq l_1\leq n_1^{-1}$ have been evaluated, and cross sections for $n_1 \geq$ have been obtained by extrapolation. The cross section for the production of $Fe^{+25}(n,1)$, is given by

$$\sigma(n,1) = \sigma_d(n,1) + \sum_{n_1=n+1}^{\infty} \sum_{l_1=0}^{n_1^{-1}} \sigma_d(n_1 l_1) B(n_1,l_1,n,1) \qquad (1)$$

where $\sigma_d(n_1,l_1)$ is the cross section for direct capture of an electron into the (n_1,l_1) state, and $B(n_1,l_1n,1)$ is the probability for radiative cascading of $Fe^{+25}(n_1,l_1)$ into $Fe^{+25}(n,1)$. The values of $B(n_1,l_1,n,1)$ are obtained using a separate program.

The results for the formation of Fe^{+25} with the final states of 1s, 2p, 2s are given in Table 1. The cross-sections are given in cm^2 per hydrogen atom in the target gas, and are weighted with the abundance listed. An interesting result that emerges from the present calculation, shown in Table 1, is that of all elements considered, atomic hydrogen contribures least to the production of the Lyman α line despite its large abundance. In particular, the contribution of O and Fe are substantially larger than other elements considered. The large contribution of elements other than atomic hydrogen is due to 2 factors. i) The strong target charge dependence of the electron capture cross section. For high

projectile energy the cross section increases as the 5th power of the effective charge of the target electrons. ii) The cross section is the sum of contribution from all target atomic shells.

These results are qualitatively similar to those obtained by Serlemitsos et al (1973). However, our cross sections are lower than theirs, on the average by a factor of 3, due to the removal of of several approximations in the formula used by these authors. The most important of these approximations are: i) leaving unmodified the Oppenheimer-Brinkman-Kramers cross sections which overestimate the experimental cross sections by a factor of 2-4; ii) neglecting the screening effect of the inactive K-shell electron; iii) assuming the branching ratio of unity for cascading of the higher states of the captured electrons to the 2p state; iv) neglecting the fact that there are 2 K-shell electrons, which makes their cross sections too small by a factor of 2 for non-hydrogenic atoms; and v) neglecting contributions of all the target atomic shells other than the K-shell. The effect of the first three approximations is to increase, and the effect of the last two is to decrease their cross sections.

Similarly, Watson (1976) uses the unmodified OBK approximation and an atomic hydrogen target. And since the formula he uses accounts for 2 electrons in the K-shell, his cross sections are larger than ours by a factor of 2 in addition to the overestimation of the unmodified OBK approximation. He also uses a branching ratio of unity.

References

Barkas, W. H., and Berger, M. J. 1964, Tables of Energy Losses and Ranges of Heavy Charged Particles, NASA SP-3013.

Bates, D. R., and Boyd, A. H. 1962, Proc. Phys. Soc. 80, 1301.

Bates, D. R. 1962, Atomic and Molecular Processes (New York: Academic Press), Ch. 14.

Brinkman, H. C., and Kramers, H. A. 1930, Proc. K. Ned. Akad. Wet. 33, 973.

Brown, R. L., and Lockman, F. J. 1975, Ap. J. (Letters) 200, L115.

Burns, D. 1964, J. Chem. Phys. 41, 1521.

Cameron, A. G. W. 1973, Space Sci. Rev. 15, 121.

Froese Fischer, C. 1966, J. Chem. Phys. 45, 1417.

Ginzburg, V. L., and Syrovatskii, S. I. 1964, The Origin of Cosmic Rays (New York: Pergamon Press), p. 122.

Hall, R. D., Meegan, C. A., Walraven, G. D., Djuth, F. T., and Haymes, R. C. 1976, Ap. J. 210, 631

Haymes, R. C., Walraven, G. D., Meegan, C. A., Hall, R. D., Djuth, F. T., and Shelton, D. H. 1975, Ap. J. 201, 593.

Hoffman, W. F., Frederick, C. L., and Emery, R. J. 1971, Ap. J. (Letters), 164, L23.

Kellogg, E., Gursky, H., Murray, S., Tananbaum, H., and Giacconi, R. 1971, Ap. J. (Letters), 169, L99.

Lingenfelter, R. E., and Ramaty, R. 1977, in The Structure and Content of the Galaxy and Galactic Gamma Rays, NASA CP-002, p. 237.

Meneguzzi, M., and Reeves, H. 1975, Astron. and Astrophys., 40, 91.

Merzbacher, E., and Lewis, H. W. 1958, Hand. Physik, 34, 186.

Messiah, A. 1966, Quantum Mechanics (New York: John Wiley).

Meyer, J. P. 1972, Astron. and Astrophys. Suppl., 7, 417.

Meyer, P., Ramaty, R., and Webber, W. 1974, Physics Today, 27, 23.

Mezger, P. G. 1974, Proc. of the ESO/SRC/CERN Conf. on Research Programmes for the New Large Telescope (Geneva), p. 79.

Nikolaev, V. S. 1967, Soviet Physics JETP, 24, 847.

Northcliffe, L. C., and Schilling, R. F. 1970, Nuclear Data (New York: Academic Press) A7, p. 233.

Olson, R. E., and Salop, A. 1976, Phys. Rev. A, 14, 579.

Omidvar, K. 1975, Phys. Rev. A, 12, 911.

Omidvar, K., Golden, J. E., McGuire, J. H., and Weaver, L. 1976, Phys. Rev. A, 13, 500.

Oppenheimer, J. R. 1928, Phys. Rev., 31, 349.

Pravdo, S., and Boldt, E. 1975, Ap. J. 200, 727.

Pravdo, S. H., Becker, R. H., Boldt, E. A., Holt, S. S., Rothschild, R. E., Serlemitsos, P. J., and Swank, J. H. 1976, Ap. J. (Letters), 206, L41.

Ramaty, R., Kozlovsky, B., and Lingenfelter, R. 1975, Space Science Rev. 18, 341.

Ramaty, R., Kozlovsky, B, and Lingenfelter, R. 1977 (in preparation).

Ramaty, R., Kozlovsky, B., and Suri, A. 1977, Ap. J. 214, 617.

Rule, D. W. 1977, Phys. Rev. A, 15.

Schiff, H. 1954, Canad, J. Phys. 32, 393.

Scoville, N. Z., Solomon, P. M., and Jefferts, K. B. 1974, Ap. J. (Letters), 187, L63.

Serlemitsos, P. J., Boldt, E. A., Holt, S. S., Ramaty, R. and Brisken, A. F. 1973, Ap. J. (Letters), 184, L1.

Serlemitsos, P. J., Smith, B. W., Boldt, E. A., Holt, S. S., and Swank, J. H. 1977, Ap. J. (Letters), 211, L63.

Watson, W. D. 1976, Ap. J. 206, 842.

Figure Captions

Fig. 1 Approximate temperature dependence of the charge exchange cross-section in a gas of solar abundances, for five energies. The cross-sections shown are for direct capture and cascade into the 2p level.

Fig. 2 Cross-sections (in cm^2/H-atom) for charge exchange by a bare iron nucleus (dashed line) and for X-ray production (solid lines) by the Kα transition following charge exchange and excitation as functions of the kinetic energy/amu of the iron ion.

Fig. 3 Equilibrium charge fractions of Fe as functions of kinetic energy/amu. The subscripts of f give the number of electrons.

Fig. 4 The X-ray line emissivity per H-atom for an energy density of 1 eV/cm^3 in fast ions between 1 and 300 MeV/amu, with abundances described in the text, as a function of the break energy E_c, labelled by spectral indices.

Fig. 5 The ratio of X-ray line emissivity to the energy deposited in the medium, calculated for the spectra given in the text. The curves are presented as in figure 4. The difference between the neutral and ionized cases is caused only by the different rates of energy losses for these two cases.

Fig. 6 The ratios of γ-ray line emissivity to the Fe X-ray line emissivity for the assumed spectra and abundances, for the broad and narrow carbon lines at 4.44 MeV and the broad iron line at 0.847 MeV. Again these results are plotted as in fig. 4.

Table 1: Values of $\frac{N_A}{N_H}\sigma_A$ in cm^2/H-atom where N_A/N_H = abundance of species A relative to hydrogen, σ_A = cross-section for formation of Fe^{+25} due to electron capture by Fe^{+26} from an atom of species A, for several values of the iron's kinetic energy/amu in MeV/amu. The cross-sections given are for direct capture plus cascade into the final state listed.

Table 2: Multiplicities, or the number of Kα X-ray photons produced by an iron ion, injected with energy E, as it loses energy in a neutral or an ionized medium. The multiplicities were calculated by using equation (6), and were assumed to be injected with the charge fractions shown in Figure 3.

TABLE 1

Element	Abundance	Final State	E = 5 MeV/amu	10	13	20	30
		1s	2.73-21	8.16-23	2.24-23	2.41-24	3.08-25
H	1.	2p	2.25-21	6.64-23	2.00-23	1.55-24	1.58-25
		2s	7.92-23	3.58-24	1.00-24	1.12-25	2.25-26
		1s	4.94-21	1.53-22	4.21-23	4.57-24	5.89-25
He	0.085	2p	4.08-21	1.24-22	3.11-23	2.94-24	3.02-25
		2s	1.46-22	6.72-24	1.90-24	2.14-25	4.29-26
		1s	4.54-21	2.15-22	6.48-23	8.14-24	1.15-24
C	3.71-4	2p	3.68-21	1.72-22	4.79-23	5.11-24	5.73-25
		2s	1.78-22	1.00-23	3.05-24	3.91-25	8.63-26
		1s	1.81-21	1.01-22	3.12-23	4.11-24	5.97-25
N	1.18-4	2p	1.48-21	7.89-23	2.27-23	2.56-24	2.96-25
		2s	7.86-23	4.72-24	1.49-24	2.01-25	4.57-26
		1s	1.91-20	1.22-21	3.93-22	5.52-23	8.30-24
O	6.76-4	2p	1.56-20	9.59-22	2.86-22	3.40-23	4.08-24
		2s	9.15-22	5.84-23	1.91-23	2.74-24	6.46-25
		1s	3.59-21	3.00-22	1.05-22	1.67-23	2.73-24
Ne	1.08-4	2p	2.90-21	2.30-22	7.47-23	1.00-23	1.29-24
		2s	2.11-22	1.45-23	5.19-24	8.64-25	2.20-25
		1s	1.46-21	1.50-22	5.63-23	1.01-23	1.82-24
Mg	3.34-5	2p	1.17-21	1.13-22	3.93-23	5.92-24	8.79-25
		2s	9.67-23	7.03-24	2.80-24	5.59-25	1.54-25
		1s	2.25-21	2.55-22	1.03-22	2.07-23	4.09-24
Si	3.14-5	2p	1.77-21	1.80-22	6.96-23	1.16-23	1.80-24
		2s	1.40-22	1.12-23	5.05-24	1.23-24	3.61-25
		1s	1.35-21	1.51-22	6.42-23	1.42-23	3.08-24
S	1.57-5	2p	1.06-21	1.07-22	4.12-23	7.60-24	1.28-24
		2s	6.76-23	7.03-24	3.38-24	9.15-25	2.83-25
		1s	6.75-21	6.62-22	2.85-22	6.51-23	1.75-23
Fe	2.61-5	2p	4.72-21	4.55-22	1.61-22	2.82-23	5.52-24
		2s	3.89-22	3.59-23	1.74-23	4.78-24	1.72-24
		1s	4.85-20	3.29-21	1.19-21	2.01-22	4.02-23
TOTALS		2p	3.87-20	2.49-21	7.94-22	1.09-22	1.62-23
		2s	2.30-21	1.59-22	6.22-23	1.20-23	3.58-24

TABLE 2

Multiplicities

E (MeV/amu)	Neutral Medium (Photons)	Ionized Medium (Photons)
2	2.0×10^{-4}	2.4×10^{-5}
4	.0296	.00414
6	.281	.0413
8	1.031	.156
10	2.32	.361
12	3.92	.620
14	5.48	.877
16	6.77	1.09
18	7.75	1.26
20	8.46	1.38
22	8.98	1.47
24	9.38	1.54
26	9.68	1.60
28	9.92	1.64
30	10.11	1.67
32	10.26	1.70
34	10.38	1.72
36	10.48	1.74
38	10.56	1.76
40	10.63	1.77

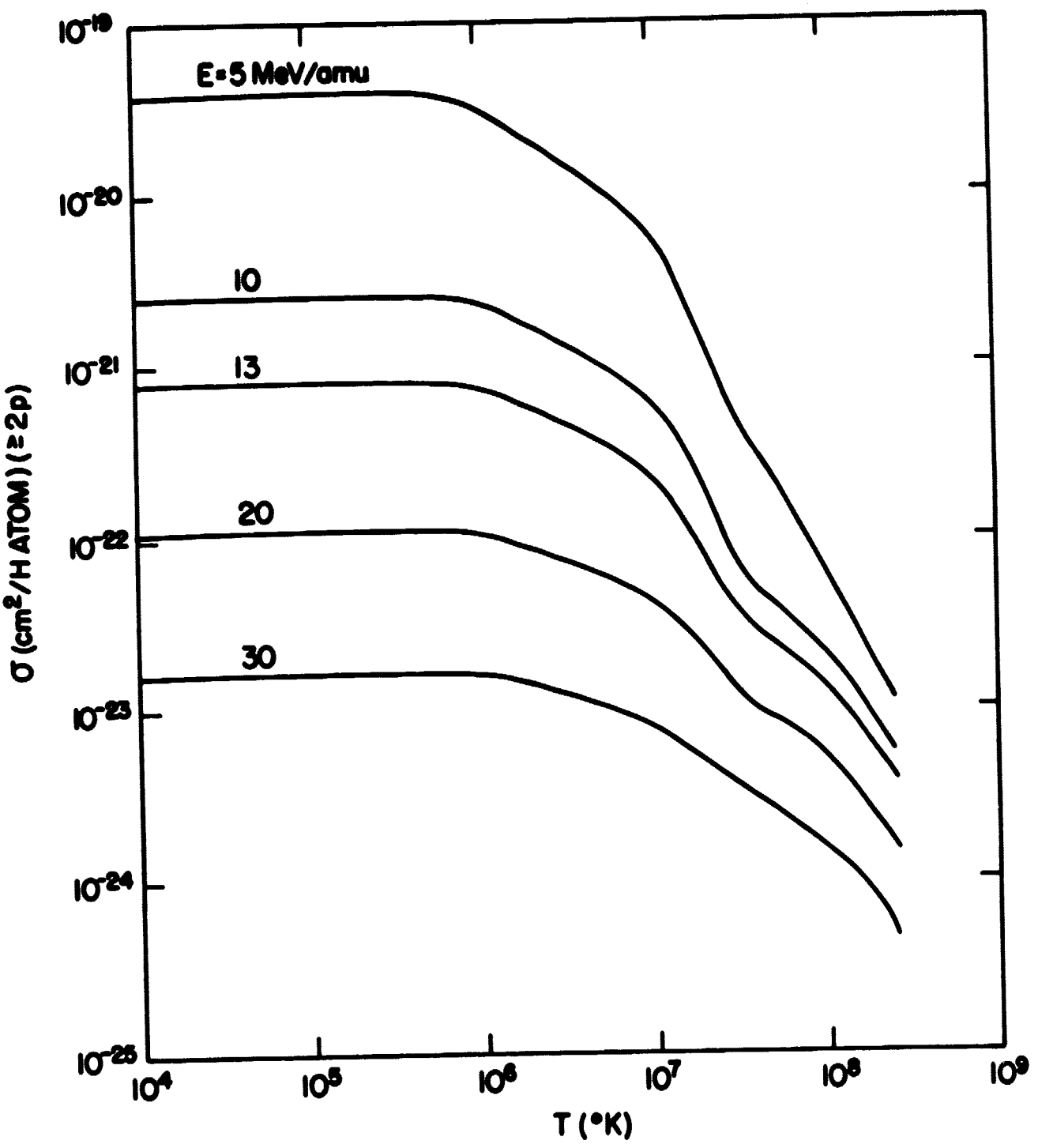
E=5 MeV/amu
10
13
20
30
σ (cm²/H ATOM) (≥2p)
T (°K)
10⁻¹⁹
10⁻²⁰
10⁻²¹
10⁻²²
10⁻²³
10⁻²⁴
10⁻²⁵
10⁴
10⁵
10⁶
10⁷
10⁸
10⁹

Figure 1

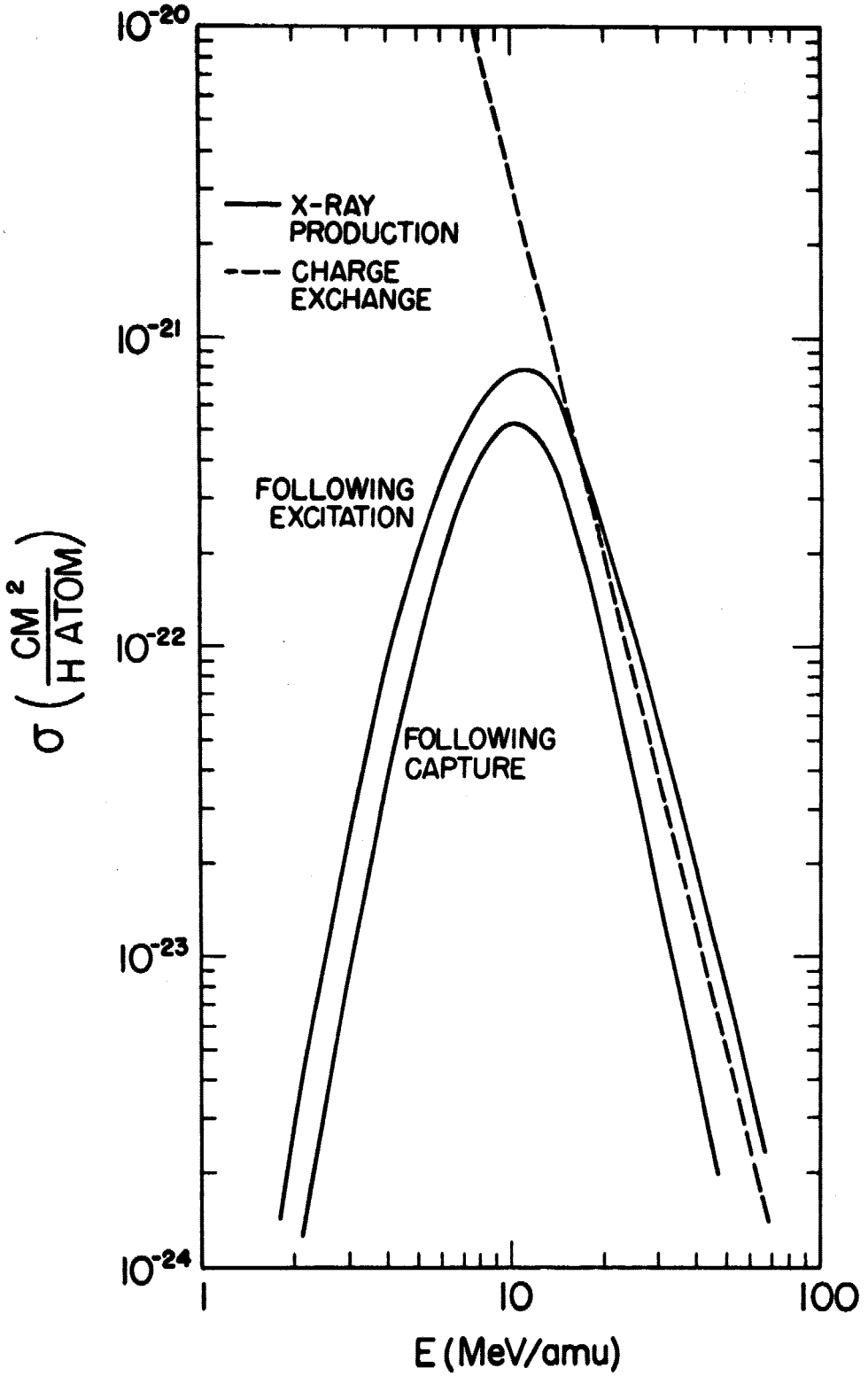
10^-20
10^-21
10^-22
10^-23
10^-24
X-RAY PRODUCTION
CHARGE EXCHANGE
FOLLOWING EXCITATION
FOLLOWING CAPTURE
σ (CM² / H ATOM)
1
10
100
E (MeV/amu)

Figure 2

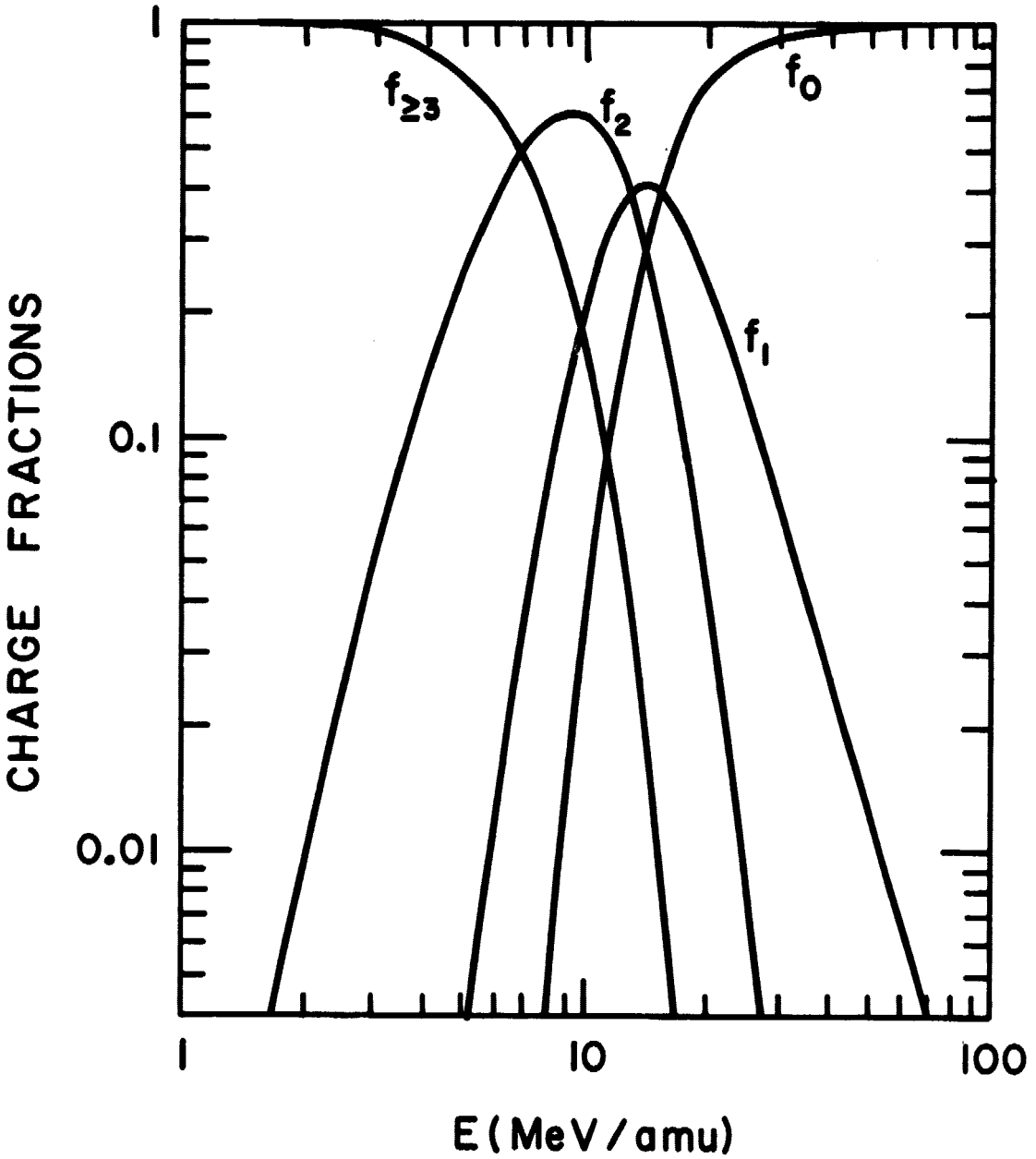

Figure 3

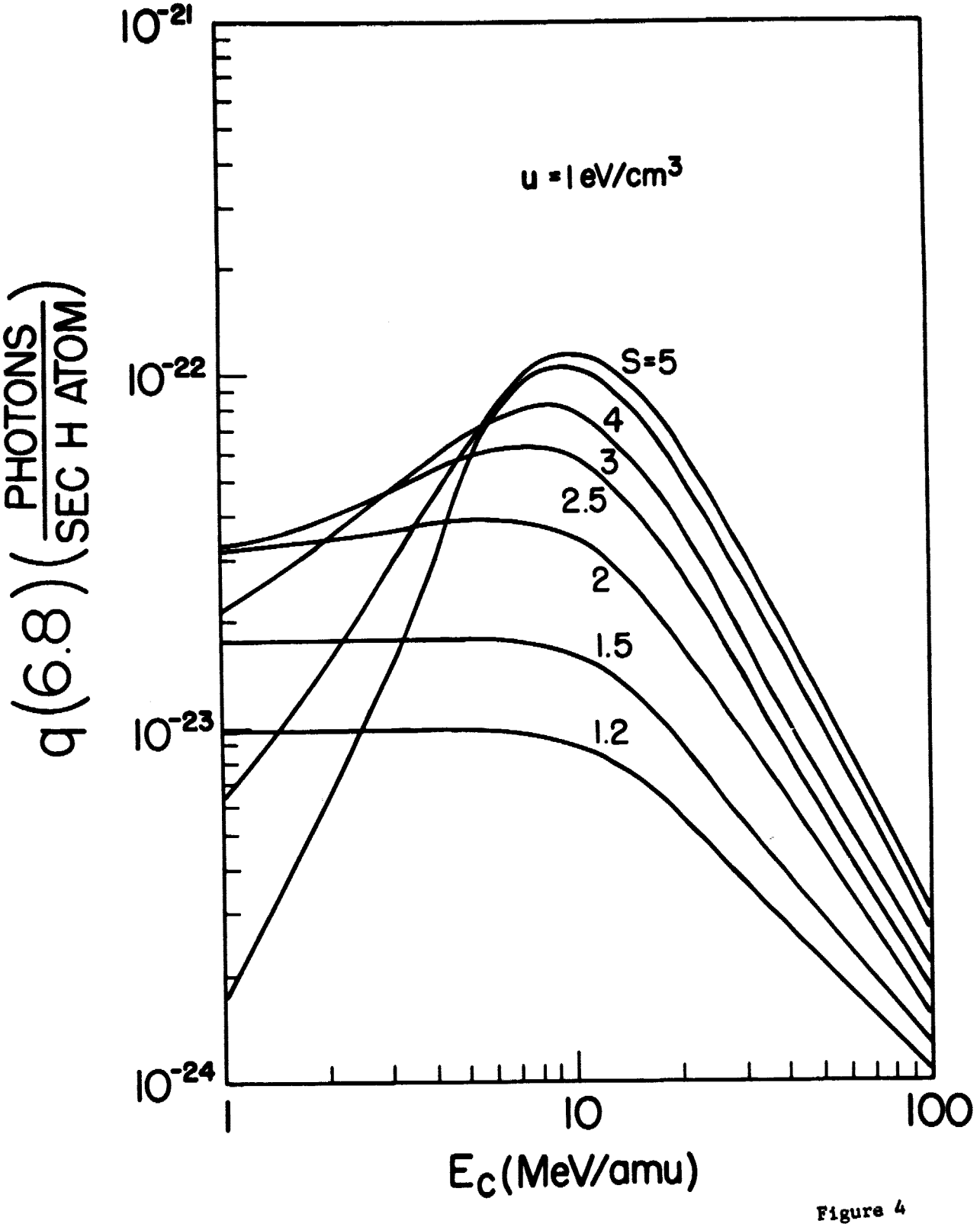
10^{-21}
10^{-22}
10^{-23}
10^{-24}
$u = 1\ eV/cm^3$
S=5
4
3
2.5
2
1.5
1.2
1
10
100
E_c(MeV/amu)
$q(6.8)\left(\frac{\text{PHOTONS}}{\text{SEC H ATOM}}\right)$

Figure 4

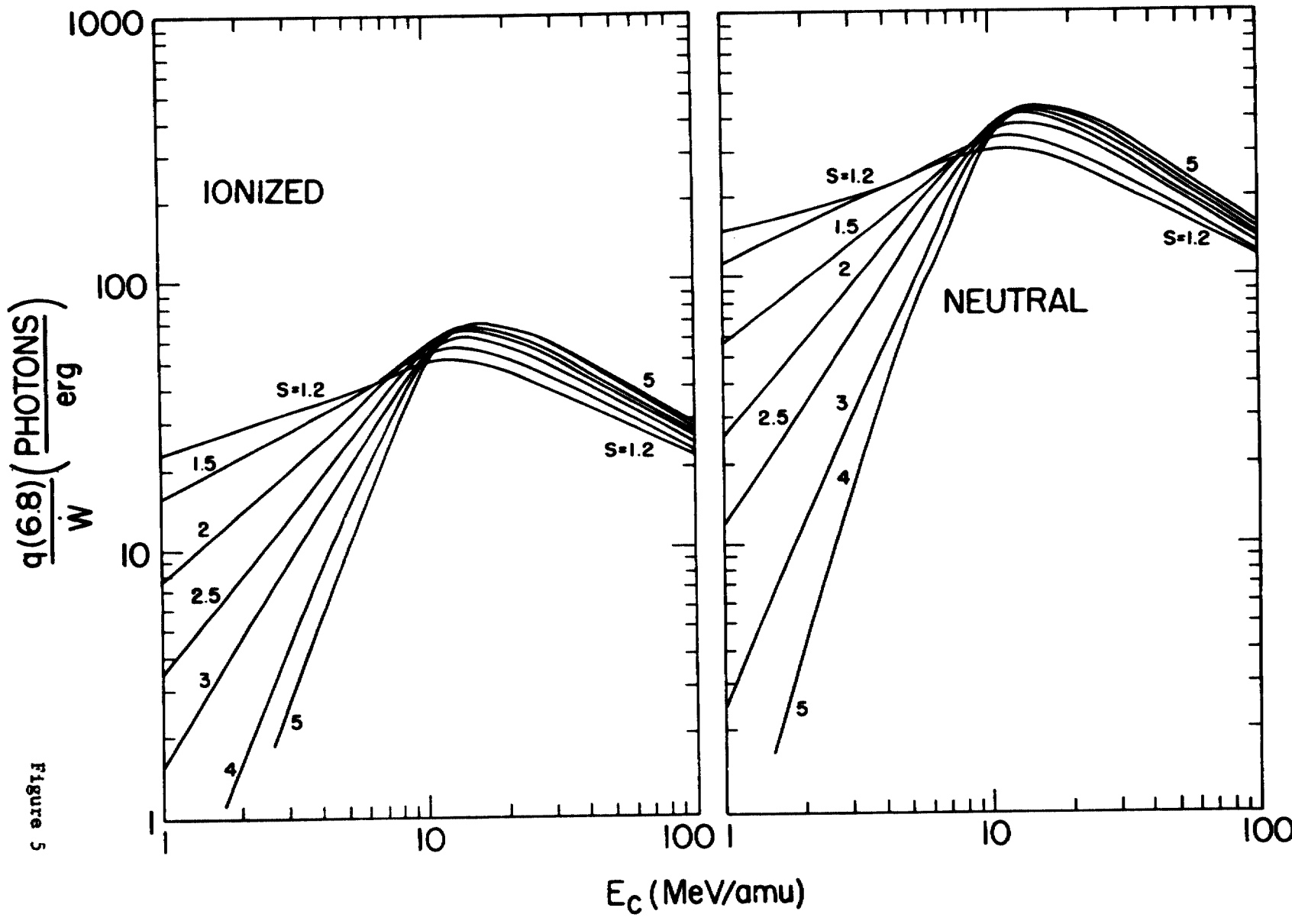
1000
100
10
1
IONIZED
NEUTRAL
S=1.2
1.5
2
2.5
3
4
5
S=1.2
5
1
10
100
$\frac{q(6.8)}{W}\left(\frac{\text{PHOTONS}}{\text{erg}}\right)$
E_c (MeV/amu)

Figure 5

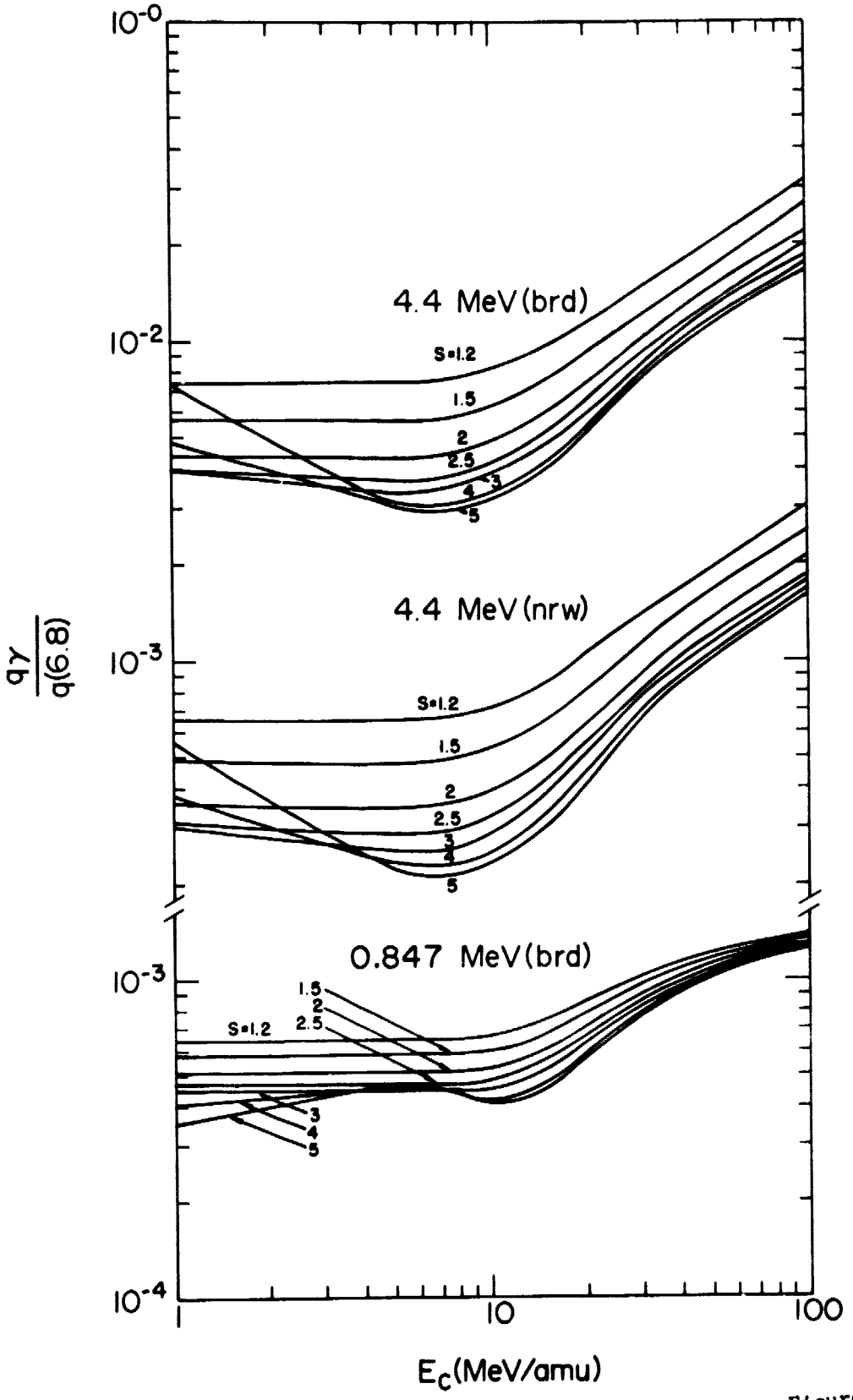
10-0
10-2
10-3
10-3
10-4
4.4 MeV(brd)
S=1.2
1.5
2
2.5
3
4
5
4.4 MeV(nrw)
S=1.2
1.5
2
2.5
3
4
5
0.847 MeV(brd)
S=1.2
1.5
2
2.5
3
4
5
1
10
100
Ec(MeV/amu)
qγ / q(6.8)

Figure 6